EurJOC
European Journal of Organic Chemistry

Research Article
doi.org/10.1002/ejoc.202300461

Chemistry Europe
European Chemical Societies Publishing

www.eurjoc.org

Special Collection

Meta-Ortho Effect on the Excited State Pathways of Chloroanilines

Cristina Nitu[+],[a, b] Jacob Jan van der Wal[+],[a] Nidhi Kaul,[a] Jorn D. Steen,[a] Leif Hammarström,[a] Maurizio Fagnoni,[c] and Stefano Crespi*[a]

Stefano Crespi was nominated to be part of this collection by EurJOC Board Members Burkhard König and Stefano Protti

Direct excitation of aromatic compounds grants access to high-energy intermediates that can be utilised in organic synthesis. Understanding and predicting the substituent effects at the excited state for aromatic molecules remains challenging for the synthetic photochemist. In this work, we present an experimental and computational investigation of the excited state of the isomeric chloroanilines, which promptly react by losing the chloride when the amino group is in *para* position, but are non-reactive and non-emissive in the *meta* and *ortho* isomers. XMS-CASPT2//CASSCF computations explain this apparent contradiction of the *meta-ortho* selectivity rule of Zimmerman, which originates from the substituent effects lowering to a different extent the barrier to populate the prefulvenic conical intersection that deactivates non-radiatively the singlet excited state of the chloroanilines.

Introduction

Photochemistry stands out among other chemical activation methods due to the possibility of spatiotemporally controlling a substrate. Photons are, by definition, the greenest of the reagents, being able to excite a molecule without leaving waste products behind and allowing reactivities unparalleled by their thermal counterparts.[1,2] While the ability to overcome potential energy barriers towards high-energy or exotic intermediates is beneficial for the success of organic photochemistry, its application is often hampered by the lack of generalised rules mirroring the depth of understanding we have reached in the (relatively) more easily explorable ground state reactions.[3,4]

[a] C. Nitu,[+] J. J. van der Wal,[+] N. Kaul, Dr. J. D. Steen, Prof. L. Hammarström, Dr. S. Crespi
Department of Chemistry – Ångström Laboratory
Uppsala University
Box 523, 751 20 Uppsala (Sweden)
E-mail: stefano.crespi@kemi.uu.se

[b] C. Nitu[+]
Stratingh Institute for Chemistry, Faculty of Science and Engineering
University of Groningen
Nijenborgh 4, 9747 AG Groningen (The Netherlands)

[c] Prof. M. Fagnoni
Department of Chemistry – PhotoGreen Lab
University of Pavia
Viale Taramelli 12, 27100 Pavia (Italy)

[+] These authors contributed equally to this work.

Supporting information for this article is available on the WWW under https://doi.org/10.1002/ejoc.202300461

Part of the #NextGenOrgChem Special Collection.

The photochemistry of aromatic compounds is extensively studied due to their ubiquitous presence in natural and artificial products.[5] A thorough effort to elucidate the photochemical deactivation pathways of benzene has been undertaken since the discovery of *conical intersections* (CoIns)[6] regulating its excited state reactivity (the nonradiative *channel 3* of benzene *vs* fluorescence decay and intersystem crossing).[7,8] More specifically, benzene can transform upon UV irradiation into its valence isomers *via* decay through several conical intersections (see Figure 1a).[5,9,10] One of them is the S_1/S_0 prefulvenic **CoIn** formed as a carbon atom of the excited singlet bends out of the ring plane and two *meta* carbons start interacting. Radiationless relaxation on the ground state surface leads to the regeneration of benzene and to fulvene and benzvalene to a minor extent (Figure 1a).[5,9]

Even recently, this side of the excited state of benzene continues to offer surprising facets.[7,11,12] Indeed, the synthetic possibilities that the excited state of small aromatics offer (e.g. for dearomatisation reactions[5] or photo-S_N1 arylations[13–15]) are bountiful and not yet fully explored. Direct excitation of aromatics can indeed be used to generate synthetically appealing intermediates.[12,16] Taming the excited state of arenes necessitates rules to predict their behaviour.

Zimmerman's work on the substituent effect on excited aromatics was a ground-breaking discovery. According to Zimmerman, electron transmission switches from a *para-ortho* selectivity in the ground state to *meta-ortho* in the excited state. (Figure 1b).[4,17] Although this effect has since been recognised, for example, in the selectivity of nitrophosphate esters photohydrolysis in aqueous solution (Figure 1b)[18] and in the solvolysis of methoxybenzyl derivatives,[19] a complete picture of substituent effects in the excited state of substituted benzenes is lacking and no general predictions can be made.

Research Article
doi.org/10.1002/ejoc.202300461

Chemistry Europe
European Chemical Societies Publishing

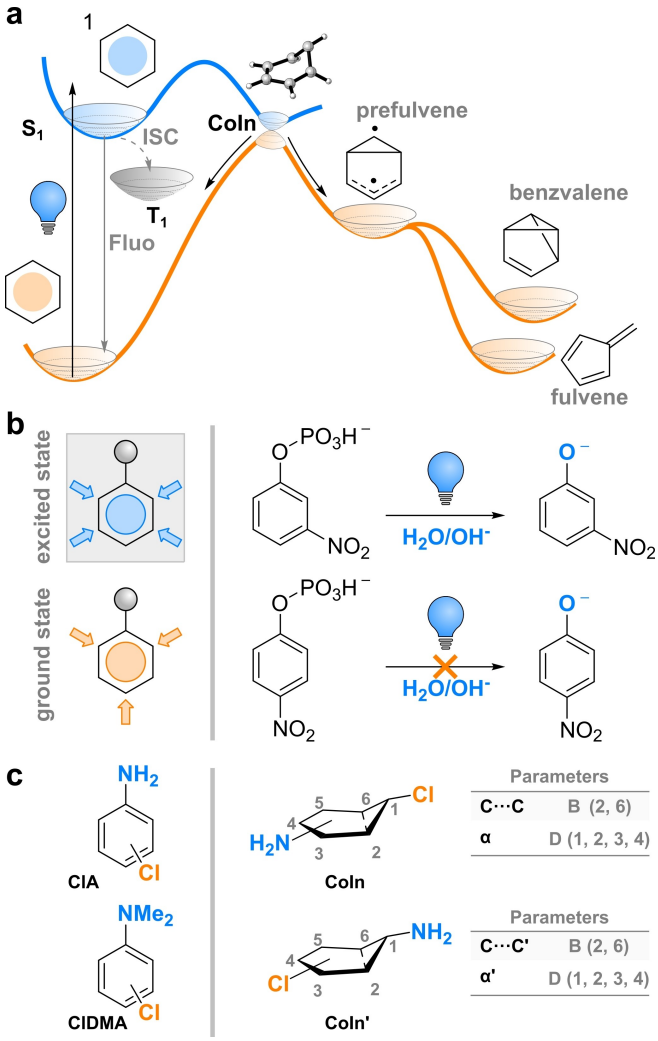

Figure 1. a) Pictorial representation of the different deactivation pathways in excited state aromatics, using benzene as a paradigmatic example. b) Ground and excited state substituent effects according to Zimmerman (left) and photochemical hydrolysis of nitrobenzylphosphonates (right). c) Molecules considered in this study and principal parameters used in the evaluation of the conical intersections.

In this general context, excited chloroanilines offer a peculiar case of selectivity. The principal deactivation mode of *p*-chloroaniline (***p*-ClA**) is the population of the triplet state and consequent heterolytic cleavage of the C–Cl bond.[15,20,21] Only a minor part of the excited state population will deactivate radiatively (see Table 1). The position of the amino group, however, appears to affect the outcome of the photochemical reaction, somehow contradicting the observation of Zimmerman. While ***p*-ClA** readily dissociates with high quantum yields, its *meta* and *ortho* (***m*-ClA** and ***o*-ClA**) counterparts are relatively stable under irradiation (Table 1) and weakly or not emissive.[22–24] This marked difference poses the question as to why only ***p*-ClA** can lose efficiently the chlorine and further react, apparently contradicting the substituent effects for enhanced photoreactivity with *meta-ortho* selectivity proposed by Zimmerman.

A suitable hypothesis is that ***m*-ClA** and ***o*-ClA** in the S_1 state are able to deactivate even before crossing to the reactive T_1 surface (see Figure 1a). The fluorescence quantum yield decreases in the order *para* > *ortho* ~ *meta* (see Table 1), excluding emission as the main decay pathway for excited ***m*-ClA** and ***o*-ClA**. Non-radiative decay is another possibility. Similarly to the benzene case, S_1/S_0 conical intersections[6] may be responsible for the ultra-fast conversion from the S_1 surface to the S_0 in chloroanilines. Prefulvenic CoIns have been identified computationally in monosubstituted benzenes such as phenol[25] and toluene[26] in which the deformation appears at the *ipso* carbon (Figure 1c). Additionally, among the four possible prefulvenic geometries of aniline with distortion at different positions, the lowest energy isomer is still puckered at the carbon bearing the amino group according to Sala et al.[27] This type of distortion has also been observed for the S_1/S_0 internal conversion of halogenated derivatives. In literature, a prefulvenic minimum energy crossing point derived from *ab initio* calculations is presented for hexafluorobenzene,[28] while photodynamics simulations on tri-, tetra-, penta- and hexafluorobenzenes indicate S_1/S_0 surface hopping points with C–F out-of-plane bending and ring puckering at the substituted carbons.[29]

By extension, the existence of prefulvenic conical intersections for chloroanilines can be hypothesized. Indeed, such geometries have been reported with puckering at the chlorine-bearing carbon (**CoIn** in Figure 1c).[30] Another possibility would be for C–N to be pushed out of the plane, as for **CoIn′** in Figure 1c, and so two pathways are opened up for the non-radiative decay of chloroanilines in the singlet excited state.

Stefano Crespi obtained his PhD in Chemistry at the University of Pavia in 2017. He spent two years as a postdoctoral fellow in Pavia, followed by a five-month period at the University of Regensburg (Germany) and two and a half years in Groningen (The Netherlands) as Marie Curie postdoctoral fellow at Ben Feringa's laboratory. In 2022, he became an assistant professor in Organic Photochemistry at Uppsala University. His main research focus is the design and mechanistic understanding of photochemical reactions and mechanical motion at the nanometer scale.

Table 1. Quantum yields of disappearance (Φ_{-1}) and fluorescence (Φ_F) for different chloroanilines.

	Φ_{-1}	Φ_F
***p*-ClA**	0.55[a][24] (0.03)[b][33]	0.019[a][24]
***m*-ClA**	0.014[a][23]	_[c][34]
o-ClA	0.048[a][22]	_[d][34]
***p*-ClDMA**	0.95[a][33] (0.05)[b][33]	0.026[a][24] (0.007)[b]
***m*-ClDMA**	<0.05[a,b]	<0.01[a,b]
o-ClDMA	<0.05[a,b]	<0.01[a,b]

[a] MeOH. [b] Cyclohexane. [c] Dioxane, 77 K. Very weak fluorescence. [d] Dioxane, 77 K. No fluorescence.

Research Article
doi.org/10.1002/ejoc.202300461

Apart from the ring puckering (characterised by the proper dihedral angles α for **CoIn** and α′ for **CoIn**′ in Figure 1c), the conical intersection structures are also characterised by a shortening of the C2–C6 distance (C···C and C···C′ in Figure 1c). Consequently, we focused on exploring computationally the ground and the first excited singlet potential energy surfaces (PES) of chloroanilines to ascertain the role of the conical intersection geometries in controlling the reactivity of the different positional isomers.

Results and Discussion

Experimental characterisation of chlorodimethylanilines

Before focusing on the computational exploration of the excited state of the anilines, we decided to investigate experimentally the behaviour of the three isomers of the *N*-methylated chloroanilines (**ClDMA**). Our strategy was deemed necessary due to the limited information found in the literature, to the best of our knowledge, on the excited state reactivity of the alkylated *meta* and *ortho* anilines (see Table 1). We considered this information crucial to exclude experimentally that the observed reactivity between the isomeric non-alkylated chloroanilines originates from another deactivation pathway, namely the photodissociation of the N–H bond or the energy dissipation through N–H vibrations. These mechanisms occur via the population of the low-lying π-3 s state of anilines which converts into a π-σ*.[31,32] Despite being optically *dark*, this state involving Rydberg orbitals can be populated when exciting the chromophores to the S_2, using a 266 nm light from a low-pressure mercury lamp, the irradiation source often used in the literature to excite these molecules.

Our fluorescence measurements, both in cyclohexane and in methanol, confirmed the marked difference of ***p*-ClDMA** compared to the *ortho*- and *meta*- derivatives (see Table 1). As in the non-alkylated compounds, the quantum yield of fluorescence (Φ_F) was negligible compared to the reported 2.6% of ***p*-ClDMA**.[24] Similar results were obtained when comparing the reactivity of the systems (Φ_{-1}, see Table 1). The quantum yield of disappearance of ***p*-ClDMA** (in MeOH, 0.95)[33] was found to be considerably larger than the ones of ***o***- and ***m*-ClDMA** (< 0.05).

The significant difference could also be observed utilizing nanosecond transient absorption spectroscopy (see Supporting Information and Figures S15–S20). Interestingly, the transient data of ***p*-ClDMA** show an emission signal of ca. one order of magnitude larger than the other two derivatives, in accordance with the difference in quantum yield. Only for the *para* derivative it was possible to observe a long-lived (half-life > 100 μs) intermediate formed immediately after the laser pulse absorbing at ca. 440 nm both in cyclohexane and methanol. These spectral features are in accordance with the ones reported for the radical cation intermediate of the dehalogenated chloroaniline[35] and confirm the difference in reactivity observed between the three isomers. Indeed, it is safe to exclude that the origin of the difference in photophysics and photochemistry of the non-alkylated anilines arises from the dissociative N–H path.

It has to be noted that the alkylation leads to an increase in reactivity in all solvents, especially for the *para*-isomer.[33] Possibly, the N–H photodissociation represents an additional parasitic path which depletes the reaction quantum yield in the different isomers, but this cannot account for the origin of the substituent effect in this class of compounds. Having established this crucial point, we proceeded to investigate the non-alkylated chloroanilines computationally.

Computational characterisation of chloroanilines

In chloroanilines, two coordinates are of interest in examining the possibilities of non-radiative decay from the S_1 state. On the one hand, the formation of the prefulvenic CoIns can be traced from the C2–C6 distances defined in Figure 1c. The structures along this S_1 trajectory have a π-π* character.[8,30] On the other hand, the evolution of the excited state while elongating the C–Cl bond can be followed to correlate the bond dissociation event in the S_1 with the prefulvenic distortion. The π-σ* state is therefore also relevant in chloroanilines.

Considering the multiconfigurational nature of the system, the geometries were pre-optimized with SA2-CASSCF/def2-TZVP at the minimal (6,6) active space, which was then successfully expanded to (8,8) by the inclusion of C–Cl σ and σ* in order to describe the C–Cl dissociation from the π-σ* state. For a more accurate portrayal of the π-π* state, we attempted to introduce one N lone pair and one Cl lone pair to the (8,8). Since anilines have a low lying Rydberg state,[31] the addition of N 3 s was also attempted to tentatively form a (12,11) space. However, the N 3 s could not be captured during the optimisation while the occupancy of the Cl p orbital was > 1.99, so these two orbitals were discarded. Adding only the N lone pair to the initial (8,8) to generate a (10,9) space resulted in an occupancy of > 1.99 for the N p orbital. It was thus decided to keep an (8,8) active space (Figure 2a) for the subsequent multi-configurational calculations on the chloroanilines and their conical intersections.

It was possible to increase the active space including the non-bonding orbitals of N and Cl, along with the 3 s Rydberg orbital of N, by averaging more states (*vide infra*), however the optimisation of the conical intersection led to the loss of the larger active space, even by averaging 12 states. We decided to use this expanded active space only to compare singlet and triplet states along the C–Cl elongation coordinate.

For each chloroaniline isomer, the conical intersection geometries **CoIn** and **CoIn**′ (Figure 1c) were optimised alongside two minima geometries corresponding to the ground state ($\mathbf{S_0}$) or first excited state ($\mathbf{S_1}$) stable structures.

Two types of conformers were identified for the conical intersections based on the orientation of the pyramidalised $-NH_2$ group with respect to the ring distortion (Figure 2b). Consequently, in **CoIn** the hydrogens of $-NH_2$ point either towards the same side as the ring puckering (**CoIn(Z)**) or towards the opposite side (**CoIn(E)**). In parallel, the $-NH_2$

Research Article
doi.org/10.1002/ejoc.202300461

Chemistry Europe
European Chemical Societies Publishing

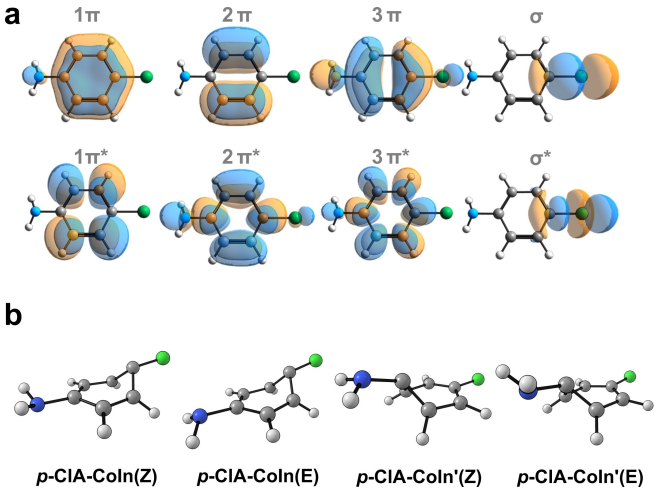

Figure 2. a) Visualization of the (8,8) active space for ***p*-ClA**–S_1.Orbitals obtained at the SA2-CASSCF/def2-TZVP level (isosurface = 0.03). b) Optimized structures of the conical intersections of ***p*-ClA** at the SA2-CASSCF/def2-TZVP level of theory.

hydrogens in **Coln′** can be oriented towards the main plane of the ring (**Coln′(Z)**), or away from it (**Coln′(E)**). In the text, the labels contain the isomer concerned (***p*-ClA**, **m-ClA**, **o-ClA**) followed by what type of structure it is (S_0, S_1, **Coln(Z)**, **Coln(E)**, **Coln′(Z)**, **Coln′(E)**).

The results of the SA2-CASSCF(8,8) optimisations are summarized in Table 2 and in the Supporting Information (see Table S2 and Figure S21). The individual active spaces along with the corresponding occupation numbers of the orbitals can be found in Figures S22–S24.

At the ground state, all the chloroaniline structures are planar with pyramidalisation at the amino group (see Figure S21). Upon excitation, the rings remain flat but the C–Cl distances become compressed by 0.01–0.02 Å (Table 1) and the C–C bonds of the benzene rings are stretched from 1.39–1.40 Å to 1.42–1.43 Å (Table S2 in the Supporting Information). The internuclear distances therefore adjust themselves in the S_1 state as a means to relieve excited state antiaromaticity.[36] The transition from the S_0 to the S_1 involves the redistribution of electrons between the π and the π* orbitals of the active space (Figures S22–S24). The occupancies of the C–Cl σ and σ* thus remain unaltered, being consistent with the nature of the vertical excitation to S_1 being π-π*.[36]

Similarly to the S_0 and S_1 minima, the relative position of the substituents has only a small effect on the prefulvenic conical intersection geometries. This is reflected in the extent of puckering. For **Coln**, the deviation from a planar benzene ring follows the *meta* < *para* < *ortho* order based on the dihedral

Table 2. Structural parameters and relative energies for the chloroaniline structures optimized with SA2-CASSCF/def2-TZVP.

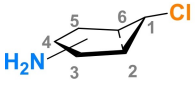

Coln

Parameters
C···C B (2, 6)
α D (1, 2, 3, 4)

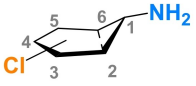

Coln'

Parameters
C···C' B (2, 6)
α' D (1, 2, 3, 4)

		ΔE_1[a] [kcal/mol]	ΔE_1[a] [eV]	ΔE_2[b] [kcal/mol]	ΔE_2[b] [eV]	ΔE_3[c] [kcal/mol]	ΔE_3[c] [eV]	C–Cl [Å]	α [deg]	C···C [Å]	α′ [deg]	C···C′ [Å]
***p*-ClA**	S_0	−107.2	−4.65					1.78	0	2.41	0	2.40
	S_1	0.0	0.00	0.0	0.00	0.0	0.00	1.76	0	2.49	0	2.49
	Coln(Z)	19.8	0.86	21.9	0.95	18.5	0.80	1.77	43	1.90		
	Coln(E)	19.9	0.86	21.9	0.95	18.5	0.80	1.77	43	1.90		
	Coln′(Z)	19.4	0.84	22.0	0.95	19.9	0.86	1.76			44	1.89
	Coln′(E)	16.0	0.69	18.5	0.80	17.0	0.74	1.76			44	1.91
***m*-ClA**	S_0	−108.1	−4.69					1.78	0	2.48	0	2.40
	S_1	0.0	0.00	0.0	0.00	0.0	0.00	1.76	0	2.43	0	2.49
	Coln(Z)	15.9	0.69	19.0	0.82	12.1	0.52	1.76	40	1.96		
	Coln(E)	16.7	0.72	20.1	0.87	12.4	0.54	1.76	40	1.96		
	Coln′(Z)	18.4	0.80	20.9	0.91	17.4	0.75	1.76			43	1.90
	Coln′(E)	15.0	0.65	17.3	0.75	14.5	0.63	1.76			42	1.92
***o*-ClA**	S_0	−108.4	−4.70					1.78	0	2.44	0	2.38
	S_1	0.0	0.00	0.0	0.00	0.0	0.00	1.76	0	2.49	0	2.47
	Coln(Z)	19.0	0.82	22.2	0.96	16.4	0.71	1.76	48	1.90		
	Coln(E)	17.0	0.74	20.2	0.88	14.4	0.62	1.77	48	1.91		
	Coln′(Z)	17.4	0.75	19.9	0.86	18.3	0.79	1.79			46	1.86
	Coln′(E)	15.6	0.68	18.0	0.78	16.8	0.73	1.78			46	1.87

[a] ΔE_1 calculated at the SA2-CASSCF/def2-TZVP level. [b] ΔE_2 calculated at the SA3-CASSCF/def2-TZVP//SA2-CASSCF/def2-TZVP level. [c] ΔE_2 calculated at the XMS3-CASPT2/def2-TZVP//SA2-CASSCF/def2-TZVP level.

angle α and the C···C distance (Table 2). The *meta* isomer therefore has the longest C···C distance, which correlates with a previous report of the **CoIn** structures optimised at the SA2-CASSCF(6,6)/6-31G(d) level.[30] The authors also report C–Cl bond lengths of 1.74–1.75 Å, slightly shorter than the **CoIn** geometries presented in this work (1.76–1.77 Å in Table 2). The difference is possibly due to the larger (8,8) active space containing the C–Cl σ and σ* orbitals combined with the more extended def2-TZVP basis set. In the other type of conical intersection, namely **CoIn′**, the distortion adopts the same *meta* < *para* < *ortho* trend. The orientation of the amino group relative to the ring puckering (**CoIn(Z)** *versus* **CoIn(E)**; **CoIn′(Z)** *versus* **CoIn′(E)**) does not influence significantly the structural parameters of the ring, nor the C–Cl bond. Energetically, the proximity of the amino group to the distortion location appears to matter only slightly due to possible steric repulsions, giving rise to small E–Z gaps between 2.0 and −3.4 kcal/mol. Nevertheless, the conformers of each conical intersection can be considered to behave similarly. Comparing the two types of conical intersections, they seem to have equivalent energies at the SA2-CASSCF(8,8) optimisation level or even if a third state is introduced to the averaging in SA3-CASSCF(8,8) single point calculations (see ΔE_1 and ΔE_2 in Table 2).

Nonetheless, adding dynamical correlation *via* XMS3-CASPT2(8,8) single point calculations leads to distinctions between the **CoIn** structures and the corresponding **CoIn′** (ΔE_3 in Table 2). For ***m*-ClA** and ***o*-ClA**, the **CoIn** geometries are slightly more favorable by 1.9–5.3 kcal/mol. Interestingly, ***p*-ClA–CoIn** and ***p*-ClA–CoIn′** are similar in energy regardless of the calculation method. As the differences between the stability of **CoIn** and **CoIn′** emerged only after the perturbational corrections, they may indicate the involvement of electronic effects from the substituents in the π-π* state even though they were not explicitly considered in the active space.

A brief analysis of the branching spaces evidences that **CoIn** and **CoIn′** structures of the chloroanilines resemble the prefulvenic conical intersection of benzene responsible for the so-called 'channel three' of S_1 deactivation (see Figure 3a, Table S3 and Figure S25 in Supporting Information). The degeneracy-lifting directions (**g** and **h**) correspond to the distortions shown in Figure 3a and they are consistent with the vectors from benzene prefulvenic conical intersections.[37] In terms of topology, all but one of the branching spaces are peaked ($P < 1$) suggesting the conical intersections can act as efficient funnels to drive internal conversion from the S_1 state to the S_0. The only one categorised as sloped (***o*-ClA–CoIn(E)**) is actually a borderline case as its P value is ~1. The *para* conical intersections are all bifurcating and so they could possibly lead to multiple products in the ground state, while the *ortho* and *meta* are all single-path suggesting the generation of only one product.

Trajectories to the prefulvenic conical intersections

Trajectories were constructed between the S_1 minima geometries and the conical intersections by generating intermediate structures and performing single point calculations with SA3-CASSCF(8,8)/def2-TZVP and XMS3-CASPT2(8,8)-def2-TZVP. The C···C and C···C′ distances were plotted against the energies of the 1st and 2nd roots resulting from the calculations as the ground state and S_1 state, respectively. All graphs are presented in Figures S26 and S27 in the Supporting Information. Transition states connecting the S_1 minima and the CoIns were optimised, apart from ***o*-ClA–CoIn(Z)** and **CoIn(E)**, where no maximum could be found. In these last cases, a minimum energy path connecting directly the conical intersection to the S_1 was computed (available in the Figshare repository provided). The energy barriers for the formation of the conical intersections from the S_1 minima are collected in Table S4.

In the ground state, the pathways from the minima to the conical intersections are equivalent between the chloroaniline positional isomers. Substituent effects, however, become noticeable on the S_1 curves (Figures 3b–d). The difference becomes more accentuated at the XMS3-CASPT2 level as the activation energies for ***m*-ClA–CoIn** result to be 12.0–12.3 kcal/mol and 14.4 kcal/mol for ***o*-ClA–CoIn(E)**, while for ***o***- and ***m*-ClA–CoIn′** they remain within the 17.0–21.9 kcal/mol range. Consequently, not only does ring puckering at the chlorine side generate conical intersections slightly lower in energy for the *m*- and *o*-chloroanilines than if the distortion was on the amino side (see previous section), it is also preferred from an energetic barrier perspective. On the other hand, there appears to be a less dramatic distinction between the generation of the two possible prefulvenic geometries from ***p*-ClA–S_1**. The barriers for both ***p*-ClA–CoIn** and ***p*-ClA–CoIn′** thus fall within 21.3–24.7 kcal/mol as computed with XMS3-CASPT2.

Subsequently, ring puckering in the vicinity of the $-NH_2$ substituent in the S_1 state has roughly the same energetic cost, regardless of which chloroaniline is under investigation (Figure 3 and Figure S27). In contrast, distortion at the chlorine-bearing atom is significantly more favorable for ***m*-ClA–S_1** and ***o*-ClA–S_1** than for ***p*-ClA–S_1**. From valence bond theory, the prefulvenic conical intersection with an S_1 electronic configuration can be considered as a diradical benzvalene structure (Figure 3e).[37] Looking at the active space occupancies of ***o*-ClA–CoIn** and ***m*-ClA–CoIn**, each of them has two orbitals with occupation numbers ~1. One has larger components on the undistorted side of the ring, while the other orbital is mainly localized on the puckered side. The same orbitals in ***p*-ClA-CoIn**, however, have less balanced occupancies (1.54 and 0.48 respectively). Consequently, it could be that varying the $-NH_2$ position on the ring leads to different interactions between the nitrogen and these two orbitals which would lead to the higher energy barrier observed in the formation of ***p*-ClA-CoIn**, leading to a long lived excited state.

C–Cl dissociation

Apart from the conical intersections, another difference among the S_1 chloroanilines could arise from the cleavage of the C–Cl bond. This coordinate was therefore varied between 1.5 and 3.50 Å for all the structures on the prefulvenic trajectories.

Research Article
doi.org/10.1002/ejoc.202300461

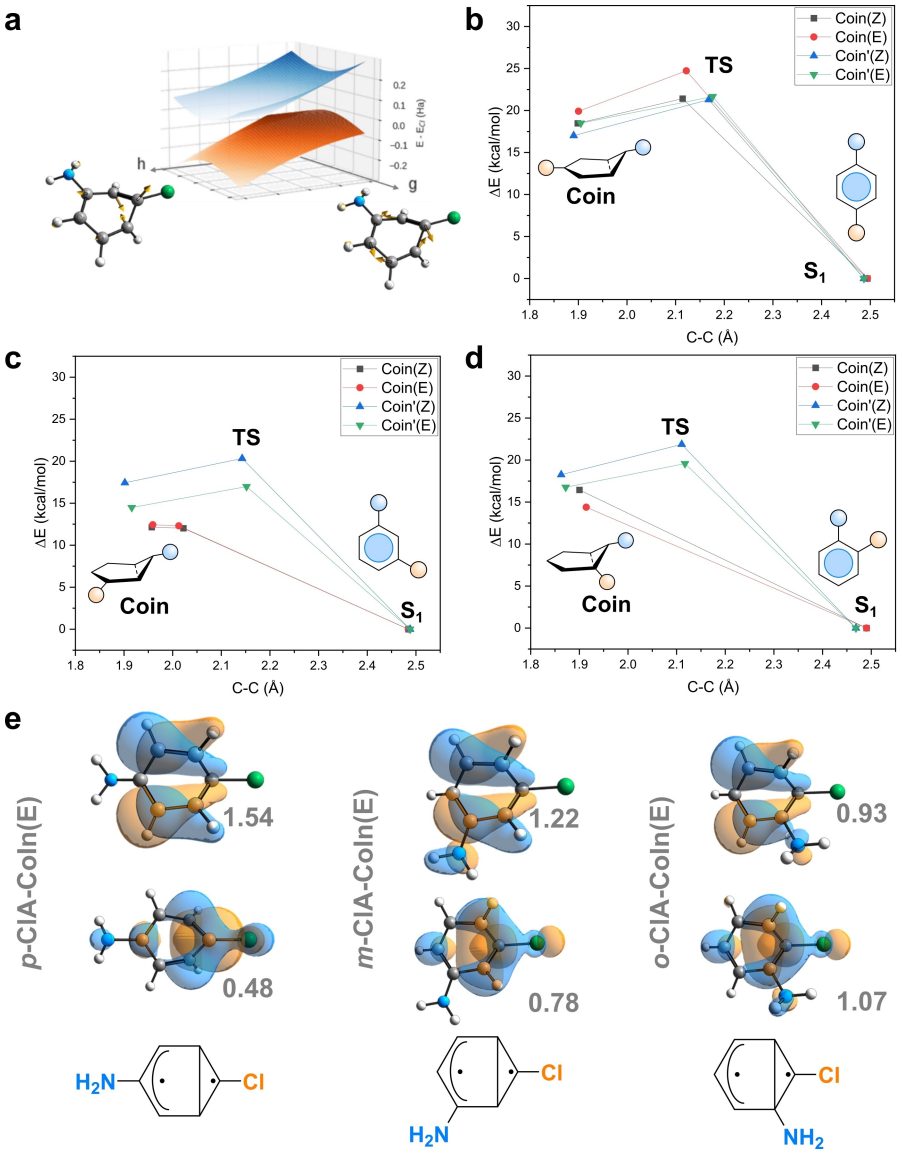

Figure 3. a) Branching space for ***m*-ClA**–**CoIn(E)**, obtained at the SA2-CASSCF(8,8)/def2-TZVP level. Energies of the different isomeric prefulvenic conical intersections in ***p*-ClA** (b), ***m*-ClA** (c) and ***m*-ClA** (d) and the corresponding transition states compared to the S_1. Energies obtained at the XMS3-CASPT2(8,8)/def2-TZVP//SA2-CASSCF(8,8)/def2-TZVP level of theory. e) Representation of the **CoIn** structures as benzvalene diradicals, along with the two active orbitals that have occupation numbers significantly smaller than 1.90 or bigger than 0.10. Orbitals obtained at the SA2-CASSCF(8,8)/def2-TZVP level (isovalue = 0.03).

Energies were extracted from single point computations in order to construct potential energy curves and surfaces. The method initially used for the optimisation of the equilibrium and conical intersection geometries – SA2-CASSCF(8,8) – broke down with the C–Cl elongation. Discontinuous dissociation curves were generated, while the active space showed signs of mixing between the π and the C–Cl σ orbitals possibly due to the π-π* and the π-σ* states being close in energy at long C–Cl distances.[36] The level of state averaging was thus increased to SA3, which partially solved the discontinuity problem. The resulting potential energy curves for C–Cl elongation are visualised in Figure S31, and the energy barriers are listed in the Supporting Information in Table S4.

While the presence of a barrier before 2.50 Å is consistent with literature on cleavage from S_1 halobenzenes[38] and chloroanilines,[30] the subsequent energy increase at distances > 2.50 Å goes against expectations. This may be a direct consequence of the rigid scan used in this project, as the previous studies allowed the structures along the C–halogen elongation coordinate to relax.[38] It could also be that the accurate portrayal of the dissociative π-σ* state requires a more extended active space and/or state averaging over more states, for instance, using SA10-CASSCF(12,10).[30] Consequently, the *meta*~*para* > *ortho* trend observed here for the energy difference between the bound and the fully dissociated geometries cannot act as unequivocal evidence for a substituent effect on the chloroaniline C–Cl cleavage.

Nevertheless, the region in Figure S31 before 2.50 Å can still be used as an indication of the chloroanilines' predisposition to undergo C–Cl elongation *versus* prefulvenic distortions in the S_1

Research Article
doi.org/10.1002/ejoc.202300461

state. At the XMS3-CASPT2(8,8) level, the dissociation from ***m*-ClA**–$\mathbf{S_1}$ (barrier of 18.6 kcal/mol) would therefore be slightly less favourable than the trajectory to the preferred conical intersection **CoIn** (barriers 12.0–12.3 kcal/mol). The reverse applies to ***o*-ClA**–$\mathbf{S_1}$ and ***p*-ClA**–$\mathbf{S_1}$, as their C–Cl cleavage barriers of 12.4 and 19.4 kcal/mol are lower than the corresponding activation energies for the generation of ***o*-ClA**–**CoIn** (14.4–16.4 kcal/mol) and ***p*-ClA**–**CoIn** (21.4–21.7 kcal/mol).

Plotting both the C–Cl bond length and the prefulvenic coordinate (*i.e.* C···C for **CoIn** or C···C′ for **CoIn′**) allows for the representation of three-dimensional PES as in Figure 4 and Figures S28–S30 in the Supporting Information. As a side note, the XMS3-CASPT2/def2-TZVP surfaces computed for pathways to ***p*-ClA**–**CoIn′(E)**, ***p*-ClA**–**CoIn′(Z)** and ***o*-ClA**–**CoIn′(E)** present discontinuities at long C–Cl distances (> 2.5 Å) and compressed C···C′ (Figures S28 and S30). Other states close in energy to the S_1 may thus be present in that region and the (8,8) active space may be unsuitable for the description of complete C–Cl dissociation from structures resembling the **CoIn′** geometries. Still, under 2.50 Å the surfaces remain relatively smooth and so the current method can be considered as a reliable descriptor for the early stages of C–Cl cleavage.

For all chloroanilines, the further the structure is on the trajectory to a conical intersection – either of the **CoIn** or the **CoIn′** type – the more disfavored the C–Cl cleavage becomes. For instance, the C–Cl elongation from the **CoIn** structures to 2.50 Å encounters a barrier of 41.9–47.4 kcal/mol at the XMS3-CASPT2(8,8) level, more than double the activation energy needed to reach the same C–Cl bond length from the S_1 equilibrium geometries. Similarly, for all the **CoIn′** geometries the barrier towards a 2.5 Å C–Cl distance falls within the 44.3–54.2 kcal/mol range.

Overall, the most significant difference between the three isomers of chloroaniline appears to stem from the **CoIn** geometries – which, interestingly, are also the preferred type of prefulvenic conical intersection in the system based on the above results. Along the C···C coordinate (i.e. distortion from the S_1 equilibrium geometry towards **CoIn**), the energy landscape of the π-π^* state is modified by the position of the amino group relative to the distorted section of the ring possibly due to different interactions between the orbitals on the nitrogen and the ring.

The trajectories to the **CoIn** structures resemble 'valleys' on the PES built in the limited coordinate space used in this work. For *m*-chloroaniline (Figure 4b), excitation from the ground state (A) leads to the first excited state minimum ***m*-ClA**–$\mathbf{S_1}$ (B). From this point (at least) three pathways are possible on the S_1 surface, namely ring puckering to form ***m*-ClA**–**CoIn** (C), C–Cl dissociation to generate D or distortion towards the other conical ***m*-ClA**–**CoIn′** (not shown in Figure 4). As the path to point C is characterised by the lowest barrier, it would be the most favoured route for the *meta* isomer. Once ***m*-ClA**–**CoIn** is reached, this geometry would ultimately mediate the non-radiative decay from the S_1 back to the S_0. The situation is similar for the *ortho* case (Figure 4c): even though the pathway towards D would be slightly more favourable than the one towards C, both the dissociation and the conical intersection

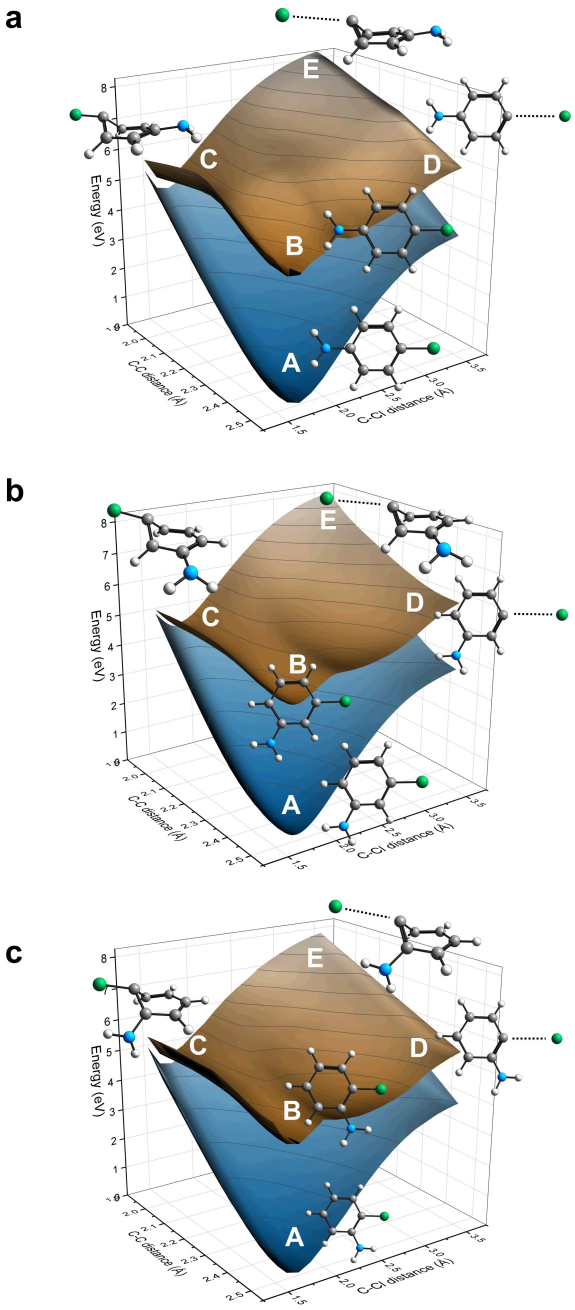

Figure 4. S_0 (blue) and S_1 (orange) surfaces describing C–Cl elongation and the formation of the **CoIn(E)** conical intersection for a) ***p*-ClA**, b) ***m*-ClA** and c) ***o*-ClA**. On each panel, points A and B correspond to the S_0 and S_1 minima. C is the respective **CoIn(E)** structure, D the fully dissociated S_1 chloroaniline (C–Cl = 3.5 Å) and E the **CoIn(E)** geometry with the C–Cl bond cleaved (C–Cl = 3.5 Å). Energies computed at the XMS3-CASPT2(8,8)//SA2-CASSCF(8,8)/def2-TZVP level.

formation have barriers under 20 kcal/mol and so S_0/S_1 internal conversion *via* ***o*-ClA**–**CoIn** remains a viable option.

The low energetic cost of forming the S_1/S_0 conical intersections in the case of *meta* and *ortho* is also consistent with these isomers being non-emissive, as they can undergo quick non-radiative deactivation, especially if the initial excitation populates a higher, more energetic excited state. Excitation

Research Article
doi.org/10.1002/ejoc.202300461

to, e.g., S_2 would indeed grant enough potential energy to overcome the barriers to access the **CoIns** at the S_1.

In contrast, the *para* S_1 minimum (point B in Figure 4a) is surrounded by barriers which are higher than for its *ortho* and *meta* counterparts in all three directions considered. Any structural distortions of ***p*-ClA**–**S_1** – and the ensuing non-adiabatic deactivation through a prefulvenic conical intersection – would be therefore slowed down. *p*-Chloroaniline would therefore be able to linger on the S_1 surface for a longer time than the *meta* and *ortho* isomers, allowing it to ultimately undergo ISC to the T_1 state, which leads to the observed photochemical reactivity.[24] All these considerations do not take into account the effect of the solvent on the barriers at the S_1. Further studies will be devoted to analysing the difference between polar and apolar media in the deactivation of chloroanilines and other haloaromatics.

We also performed a rigid scan of the C–Cl bond (see Figures S32–S35) to obtain a qualitative understanding of the energy difference between triplets and singlet states using single points with a larger active space (see Figure S31). The stability of the active space was maintained by averaging a larger number of states than the ones previously used, employing the XMS12-CASPT2(14,12)/def2-TZVP//SA2-CASSCF(8,8)/def2-TZVP level of theory. The difference in energy between the S_1 in the different anilines and their two lower triplet states[32] is quite similar when comparing C–Cl bonds near the S_1 minimum. These results are in accordance with our hypothesis that the difference in behaviour among the anilines is on the singlet surface and not in the accessibility of the triplets.

Conclusions

Excited state singlet chloroanilines were modelled to explore the theoretical basis for the different photochemistry observed experimentally for the *para*, *meta* and *ortho* isomers. It was proposed that the source of the diverging reactivity precedes the C-Cl dissociation happening on the triplet surface and even the ISC to the T_1 state. Prefulvenic conical intersections were therefore considered as actors in the non-radiative decay from the S_1 state. Interestingly, the increased reactivity of *p*-chloroaniline towards the substitution of the chlorine in a photo-solvolysis or reduction reaction appears to be caused by a decreased activity on the S_1 PES. Three possible pathways on the S_1 surface, namely distortion along two prefulvenic coordinates and elongation of the C–Cl bond, are partially blocked for the *para* compound as the S_1 minimum geometry is surrounded by large energetic barriers. Crossing to the T_1 surface is consequently enabled from the stable S_1 structure. In contrast, the *meta* and *ortho* compounds present a higher potential to decay non-adiabatically from S_1 to the ground state. The prefulvenic conical intersection consequently acts as a trap for the first excited singlets of *o*- and *m*-chloroaniline, preventing them from reaching the reactive triplet surface.

The distinctions between the transformation of the three S_1 chloroanilines into the two types of conical intersections considered (i.e. with puckering at the amino side or at the chlorine side) were reasoned on the basis of interactions between the substituents with the distorted π orbital system of the ring. Nevertheless, a more in-depth analysis is required to ascertain the exact nature of these substituent effects which could be done by locating and characterising the transition states of the prefulvenic trajectories. Solvent effects, as well as a larger active space or other types of multiconfigurational methods – such as MCPDFT – could also shed light on the exact influence of the $-NH_2$ group on the formation of the conical intersections.

Experimental Section

Synthesis and characterization

All synthetic, spectroscopic details and compound characterisation data can be found in the Supporting Information.

Computational Analysis

Complete active space self-consistent field (CASSCF) and second order extended multistate multiconfigurational perturbation theory (XMS-CASPT2) calculations were performed with OpenMolcas 20.10 and 22.02,[39,40] with an (8,8) active space consisting of 3 π, 3 π*, 1 σ_{C-Cl} and 1 σ^*_{C-Cl} orbitals. For the optimisation, state average over two states was used (SA2-CASSCF), while three or twelve states were used for the XMS treatment (XMS-CASPT2). For the latter case, a larger active space was chosen, including the two n orbitals of Cl, the n orbital of N and the 3 s Rydberg orbital of N. In all cases, def2-TZVP, which was previously benchmarked for similar compounds, was chosen as basis set.[15] The Resolution of identity with auxiliary basis set (RICD) was used to approximate the two-electron integrals.[41] For the perturbational treatment, IPEA shifts were set to 0, while the Imaginary Shift in the energy denominator was set to 0.05.[42] The reference weights of the XMS3- and XMS12-CASPT2 solutions were checked to avoid the presence of any intruder state. The performance of XMS3-CASPT2(8,8)/def2-TZVP//SA2-CASSCF(8,8)/def2-TZVP can be compared with other methods in Table 3. Indeed, our approximated approach performs similarly to different functionals in retrieving the first two vertical transitions of ***p*-ClA**, providing slightly lower transition energies than CAM-B3LYP. While all functionals chosen give similar results, EOM-CCSD/cc-PVTZ

Table 3. Comparison of computed vertical transition energies of ***p*-ClA**.[a]

	$S_0 \rightarrow S_1$ eV	$S_0 \rightarrow S_2$ eV
EOM-CCSD/cc-pVTZ	5.95	6.18
CAM-B3LYP/def2-TZVP	4.90	5.79
ωB97x-D3/def2-TZVP	4.98	5.90
M06-2X/def2-TZVP	4.97	5.87
SA3-CASSCF(8,8)/def2-TZVP	4.78	7.45
XMS3-CASPT2(8,8)/def2-TZVP	4.40	5.56
SA3-CASSCF(14,12)/def2-TZVP	4.81	6.21
XMS3-CASPT2(14,12)/def2-TZVP	4.15	5.85
exp. (Hexane)[45]	4.04	4.96

[a] Ground state geometry optimized at the SA2-CASSCF(8,8)/def2-TZVP level.

overshoots the transition energies compared to the DFT methods and even more significantly the experimental values. As expected, the second transition using CASSCF is found at higher energies, showing the necessity to perform a second-order correction. Interestingly, the first transition is comparable between CASSCF and CASPT2, possibly due to the localization of the excitation on the orbital of the active space chosen.

Additional figures representing the chosen active spaces can be found in the Supporting Information. Nudged elastic band image-dependent pair potential (NEB-IDPP) computations, DFT and EOM-CCSD calculations were performed with ORCA 5.0.3.[43,44]

Three dimensional S_0 and S_1 potential energy surfaces of the chloroanilines were modelled through rigid scans along two coordinates, namely the C···C (or C···C′) distance characterising the conical intersection structures and the C–Cl bond length. Firstly, S_0 and S_1 minima along with S_1/S_0 prefulvenic conical intersections were optimised with CASSCF(8,8)/def2-TZVP by averaging over two states. Pathways between the S_1 minima and the conical structures were estimated using the NEB-IDPP keyword in ORCA. For each trajectory, fifteen points were taken into consideration. Next, the C–Cl bond of each geometry was distorted between ~1.5 and 3.5 Å in 17 steps. Energies were extracted from single point calculations with SA3-CASSCF (8,8) and XMS3-CASPT2.

Supporting Information

The authors have cited additional references within the Supporting Information.[46–48]

Author Contributions

C.N. performed all computational work and wrote the preliminary draft of the manuscript, J.J.v.d.W. performed synthesis, photophysical characterisation, quantum yield determination and wrote the preliminary draft, N.K. performed laser flash photolysis experiments, J.D.S. supported the photophysical characterisation and provided funding, L.H. provided scientific equipment and infrastructure, M.F. provided the results of preliminary experiments, S.C. wrote the draft, supported the photophysical characterization, and provided funding and supervision. All authors discussed the results and agreed to the final version of the manuscript.

Acknowledgements

The authors thank Prof. H. Ottosson, Prof. D. Dondi, Prof. S. Protti and Prof. D. Ravelli for fruitful discussions. S.C. thanks the Swedish Vetenskapsrådet for a Starting Grant (2021-05414) and the Göran Gustafsson Stiftelse. J.D.S. thanks the Wenner-Gren Stiftelserna for a postdoctoral stipend (UPD2022-0079). We thank the Swedish National Infrastructure for Computations (SNIC) for a Small Compute Grant (SNIC 2022/22-525). C. N. thanks Erasmus + and the Backer foundation at the University of Groningen for mobility grants.

Conflict of Interests

The authors declare no conflict of interest.

Data Availability Statement

The data supporting the findings of this study are openly available in the supplementary material of this article and in the Figshare repository, at DOI 10.6084/m9.figshare.22788476.

Keywords: Aromatic substitution · Substituent effects · Computational chemistry · Conical intersections · Photochemistry

[1] N. J. Turro, V. Ramamurthy, J. C. Scaiano, *Modern Molecular Photochemistry of Organic Molecules*, University Science Books, Sausalito, **2010**.
[2] P. Klán, J. Wirz, *Photochemistry of Organic Compounds*, Wiley, Chichester, UK, **2009**.
[3] I. V. Alabugin, *Stereoelectronic Effects*, Wiley, Chichester, UK, **2016**.
[4] H. E. Zimmerman, *J. Phys. Chem. A* **1998**, *102*, 5616–5621.
[5] T. Slanina, R. Ayub, J. Toldo, J. Sundell, W. Rabten, M. Nicaso, I. Alabugin, I. Fdez. Galván, A. K. Gupta, R. Lindh, A. Orthaber, R. J. Lewis, G. Grönberg, J. Bergman, H. Ottosson, *J. Am. Chem. Soc.* **2020**, *142*, 10942–10954.
[6] Y. Boeije, M. Olivucci, *Chem. Soc. Rev.* **2023**, *52*, 2643–2687.
[7] R. S. Minns, D. S. N. Parker, T. J. Penfold, G. A. Worth, H. H. Fielding, *Phys. Chem. Chem. Phys.* **2010**, *12*, 15607.
[8] I. J. Palmer, I. N. Ragazos, F. Bernardi, M. Olivucci, M. A. Robb, *J. Am. Chem. Soc.* **1993**, *115*, 673–682.
[9] J. Dreyer, M. Klessinger, *Chem. Eur. J.* **1996**, *2*, 335–341.
[10] E. Pieri, D. Lahana, A. M. Chang, C. R. Aldaz, K. C. Thompson, T. J. Martínez, *Chem. Sci.* **2021**, *12*, 7294–7307.
[11] H. E. Zimmerman, *J. Am. Chem. Soc.* **1995**, *117*, 8988–8991.
[12] V. Dichiarante, D. Dondi, S. Protti, M. Fagnoni, A. Albini, *J. Am. Chem. Soc.* **2007**, *129*, 5605–5611.
[13] *Handbook of Synthetic Photochemistry*, (Eds.: A. Albini, M. Fagnoni), Wiley, **2009**.
[14] S. Witzel, M. Hoffmann, M. Rudolph, M. Kerscher, P. Comba, A. Dreuw, A. S. K. Hashmi, *Cell Rep. Phys. Sci.* **2021**, *2*, 100325.
[15] C. Nitu, S. Crespi, *J. Phys. Org. Chem.* **2023**, *36*, e4437.
[16] L. Zhang, E. M. Israel, J. Yan, T. Ritter, *Nat. Synth.* **2022**, *1*, 376–381.
[17] H. E. Zimmerman, *Pure Appl. Chem.* **2006**, *78*, 2193–2203.
[18] E. Havinga, R. O. de Jongh, W. Dorst, *Recl. Trav. Chim. Pays-Bas* **1956**, *75*, 378–383.
[19] H. E. Zimmerman, V. R. Sandel, *J. Am. Chem. Soc.* **1963**, *85*, 915–922.
[20] C. Raviola, D. Ravelli, S. Protti, A. Albini, M. Fagnoni, *Synlett* **2015**, *26*, 471–478.
[21] V. Dichiarante, S. Protti, M. Fagnoni, *J. Photochem. Photobiol. A* **2017**, *339*, 103–113.
[22] K. Othmen, P. Boule, *J. Photochem. Photobiol. A* **2000**, *136*, 79–86.
[23] K. Othmen, P. Boule, C. Richard, *New J. Chem.* **1999**, *23*, 857–861.
[24] M. Freccero, M. Fagnoni, A. Albini, *J. Am. Chem. Soc.* **2003**, *125*, 13182–13190.
[25] O. P. J. Vieuxmaire, Z. Lan, A. L. Sobolewski, W. Domcke, *J. Chem. Phys.* **2008**, *129*, 224307.
[26] S. Cogan, Y. Haas, S. Zilberg, *J. Photochem. Photobiol. A* **2007**, *190*, 200–206.
[27] M. Sala, O. M. Kirkby, S. Guérin, H. H. Fielding, *Phys. Chem. Chem. Phys.* **2014**, *16*, 3122–3133.
[28] J. M. Cox, M. Bain, M. Kellogg, S. E. Bradforth, S. A. Lopez, *J. Am. Chem. Soc.* **2021**, *143*, 7002–7012.
[29] J. Li, S. A. Lopez, *Chem. Eur. J.* **2022**, *28*, e202200651.
[30] S. Crespi, Computational Study on the Excited State Deactivation Mechanism of the Chloroanilines, **2018**.
[31] G. M. Roberts, C. A. Williams, J. D. Young, S. Ullrich, M. J. Paterson, V. G. Stavros, *J. Am. Chem. Soc.* **2012**, *134*, 12578–12589.

[32] A. O. Lykhin, D. G. Truhlar, L. Gagliardi, *J. Am. Chem. Soc.* **2021**, *143*, 5878–5889.
[33] B. Guizzardi, M. Mella, M. Fagnoni, M. Freccero, A. Albini, *J. Org. Chem.* **2001**, *66*, 6353–6363.
[34] T. K. Pal, G. K. Mallik, S. Laha, K. Chatterjee, T. Ganguly, S. B. Banerjee, *Spectrochim. Acta Part A* **1987**, *43*, 853–859.
[35] I. Manet, S. Monti, G. Grabner, S. Protti, D. Dondi, V. Dichiarante, M. Fagnoni, A. Albini, *Chem. Eur. J.* **2008**, *14*, 1029–1039.
[36] R. Papadakis, H. Ottosson, *Chem. Soc. Rev.* **2015**, *44*, 6472–6493.
[37] L. Blancafort, M. A. Robb, *J. Chem. Theory Comput.* **2012**, *8*, 4922–4930.
[38] O. A. Borg, Y.-J. Liu, P. Persson, S. Lunell, D. Karlsson, M. Kadi, J. Davidsson, *J. Phys. Chem. A* **2006**, *110*, 7045–7056.
[39] F. Aquilante, J. Autschbach, A. Baiardi, S. Battaglia, V. A. Borin, L. F. Chibotaru, I. Conti, L. De Vico, M. Delcey, I. Fdez. Galván, N. Ferré, L. Freitag, M. Garavelli, X. Gong, S. Knecht, E. D. Larsson, R. Lindh, M. Lundberg, P. Å. Malmqvist, A. Nenov, J. Norell, M. Odelius, M. Olivucci, T. B. Pedersen, L. Pedraza-González, Q. M. Phung, K. Pierloot, M. Reiher, I. Schapiro, J. Segarra-Martí, F. Segatta, L. Seijo, S. Sen, D.-C. Sergentu, C. J. Stein, L. Ungur, M. Vacher, A. Valentini, V. Veryazov, *J. Chem. Phys.* **2020**, *152*, 214117.
[40] I. Fdez. Galván, M. Vacher, A. Alavi, C. Angeli, F. Aquilante, J. Autschbach, J. J. Bao, S. I. Bokarev, N. A. Bogdanov, R. K. Carlson, L. F. Chibotaru, J. Creutzberg, N. Dattani, M. G. Delcey, S. S. Dong, A. Dreuw, L. Freitag, L. M. Frutos, L. Gagliardi, F. Gendron, A. Giussani, L. González, G. Grell, M. Guo, C. E. Hoyer, M. Johansson, S. Keller, S. Knecht, G. Kovačević, E. Källman, G. Li Manni, M. Lundberg, Y. Ma, S. Mai, J. P. Malhado, P. Å. Malmqvist, P. Marquetand, S. A. Mewes, J. Norell, M. Olivucci, M. Oppel, Q. M. Phung, K. Pierloot, F. Plasser, M. Reiher, A. M. Sand, I. Schapiro, P. Sharma, C. J. Stein, L. K. Sørensen, D. G. Truhlar, M. Ugandi, L. Ungur, A. Valentini, S. Vancoillie, V. Veryazov, O. Weser, T. A. Wesołowski, P.-O. Widmark, S. Wouters, A. Zech, J. P. Zobel, R. Lindh, *J. Chem. Theory Comput.* **2019**, *15*, 5925–5964.
[41] F. Aquilante, R. Lindh, T. Bondo Pedersen, *J. Chem. Phys.* **2007**, *127*, 114107.
[42] J. P. Zobel, J. J. Nogueira, L. González, *Chem. Sci.* **2017**, *8*, 1482–1499.
[43] F. Neese, F. Wennmohs, U. Becker, C. Riplinger, *J. Chem. Phys.* **2020**, *152*, 224108.
[44] F. Neese, *WIREs Comput Mol Sci.* **2022**, *12*, e1606.
[45] I. Iweibo, R. A. Oderinde, J. A. Faniran, *Spectrochim. Acta Part A* **1982**, *38*, 1–7.
[46] A. G. Giumanini, G. Chiavari, M. M. Musiani, P. Rossi, *Synthesis* **1980**, *1980*, 743–746.
[47] H. Reed, T. R. Paul, W. J. Chain, *J. Org. Chem.* **2018**, *83*, 11359–11368.
[48] Y. Lv, Y. Zheng, Y. Li, T. Xiong, J. Zhang, Q. Liu, Q. Zhang, *Chem. Commun.* **2013**, *49*, 8866–8868.

Manuscript received: May 13, 2023
Revised manuscript received: September 4, 2023
Accepted manuscript online: September 12, 2023
Version of record online: September 20, 2023